TABLE I. Clinical Manifestations of Reported Cases of 20q11–q12 Deletion

	Calliers' case (4 y, female)	Iqbals' case (2 y, male)	Present case (18 m, male)
General			
Growth retardation	+	+	+
Developmental delay	+	+	+
Autistic behavior	+	+	+
Sensory abnormalities/self-injury	+	+	+
Feeding difficulties	+	+	+
Gastroesophageal reflux	+	+	+
Gastrointestinal abnormalities	+ (Pyloric stenosis)	−	+ (Esophageal hiatus hernia)
Feeding intolerance	+ (Diarrhea, vomiting)	−	−
Dysphagia			+
Food refusal	+		+
Muscle tone	Hypertonia	Normal tone except for difficulty in extending the hips	Normal tone
Hearing loss		+	+
Congenital heart defect	−	−	+
Seizure/epilepsy		−	+
Central nervous system			
Cerebral atrophy	+	+	+
Craniofacial			
Triangular face	+	+	+
Hypertelorism	+	+	+
Hypoplastic alae nasi	+	+	+
Sparse hair	+		+
Down-slanting palpebral fissures	+		+
Long columella	+		+
Short, well-defined philtrum	+		+
Thin lips	+		+
Microretrognathia	+		+
Low-set ears	+		+
Extremities			
Arthrogryposis			+
Preaxial polydactyly			+
Clinodactyly of 5th fingers	+		+
Talipes equinovarus		+	
Talopes valgus			+
Ocular			
Retinal dysplasia			+
Microphthalmia		+	−
Duane anomaly		+	n.d.
Strabismus	+		−
Others			
Genital anomlies		+	−

Shadow indicates common features among three cases. y, year(s); m, month(s); +, positive; −, negative; n.d., not determined.

junction PCRs denied the deletion in parental samples (FISH data not shown and Fig. 2B by PCR using primers A, B, and C [primer B: 5′-AGC TGC TCA AAG TGG GGT ATT CTG G-3′]).

DISCUSSION

In this study, we precisely analyzed the 6.5-Mb deletion at 20q11.2–q12 in a boy, presenting with abnormal hands and feet, retinal dysplasia, and intractable feeding difficulty. Proximal interstitial deletions of 20q11–q12 are very rare. Only two cases have been reported and analyzed either by chromosomal CGH and FISH analysis or BAC array CGH with 1-Mb resolution [Callier et al., 2006; Iqbal and Al-Owain, 2007]. Clinical features are presented in Figure 1 and summarized in Table I. Three deletions are overlapping and the shortest region of overlap is from 20q11.22 to q11.23 (Fig. 3). Common clinical features among three cases are

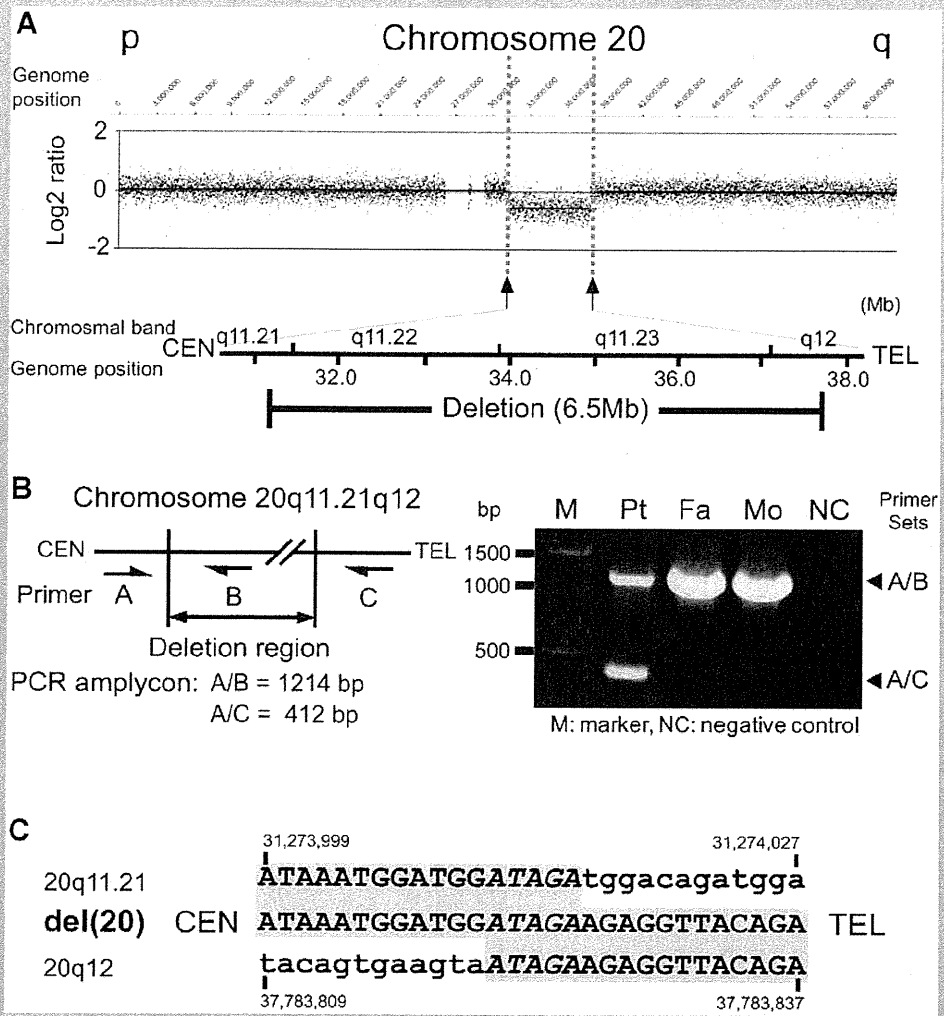

FIG. 2. Analysis of the 20q11.21–q12 deletion. A: High-resolution SNP array revealed the 6.5-Mb deletion at 20q11.21–q12. In the upper part, *Y* and *X* axes indicate probe signal intensity (log 2 ratio) and probe position in chromosome 20, respectively, and in the lower, chromosomal bands together with location of the deletion are shown. B: PCR system (left) to delineate the deletion and its result (right). C: Deletion junction sequence. Upper and lower sequences are normal ones around at proximal [20q11.21] and distal [20q12] deletion breakpoints, respectively. Middle shows the deletion junction in the patient. Gray shadow indicates matched sequences.

growth/developmental retardation, intractable feeding difficulties with GER, cerebral atrophy, and dysmorphic face including triangular face, hypertelorism, and hypoplastic alae nasi. In addition, two out of three patients shared many other facial dysmorphism including sparse hair, downslanting palpebral fissures, long columella, short and well-defined philtrum, thin lips, microretrognathia, and low-set ears. These findings suggest that the 20q11.22–q11.23 deletion can be a recognizable microdeletion syndrome. In addition, unique findings of hands and feet abnormalities as well as retinal dysplasia were found in our patient.

Intractable feeding difficulties in the three patients, is the largest concern for the family, and are speculated to be caused by combined factors: prolonged dysphagia (in our case), aspiration associated with GER (in all three), upper gastrointestinal tract abnormalties (pyloric stenosis [Callier et al., 2006] or esophageal hiatus hernia in our case), vomiting/diarrhea because of feeding intorerance [Callier et al., 2006], sensory abnormalities (in all), and food refusal (in the Callier et al. and our patient).

According to UCSC genome browser (March 2006 assembly), the 6.5-Mb deleted segment identified in our patient encompasses at least 96 known genes, including nine genes related to human disorders. One of these is growth/differentiation factor-5 (*GDF5*, also known as *CDMP1*). This is a protein which belongs to the GDF-subgroup of BMPs and plays an key regulatory role in embryonic skeletal and joint development. *GDF5* abnormalities are known to cause a variety of different skeletal disorders. Interestingly, Everman et al. [2002] and Yang et al. [2008] indicated that functional *GDF5* haploinsufficiency was the culprit of brachydactyly type C (BDC,

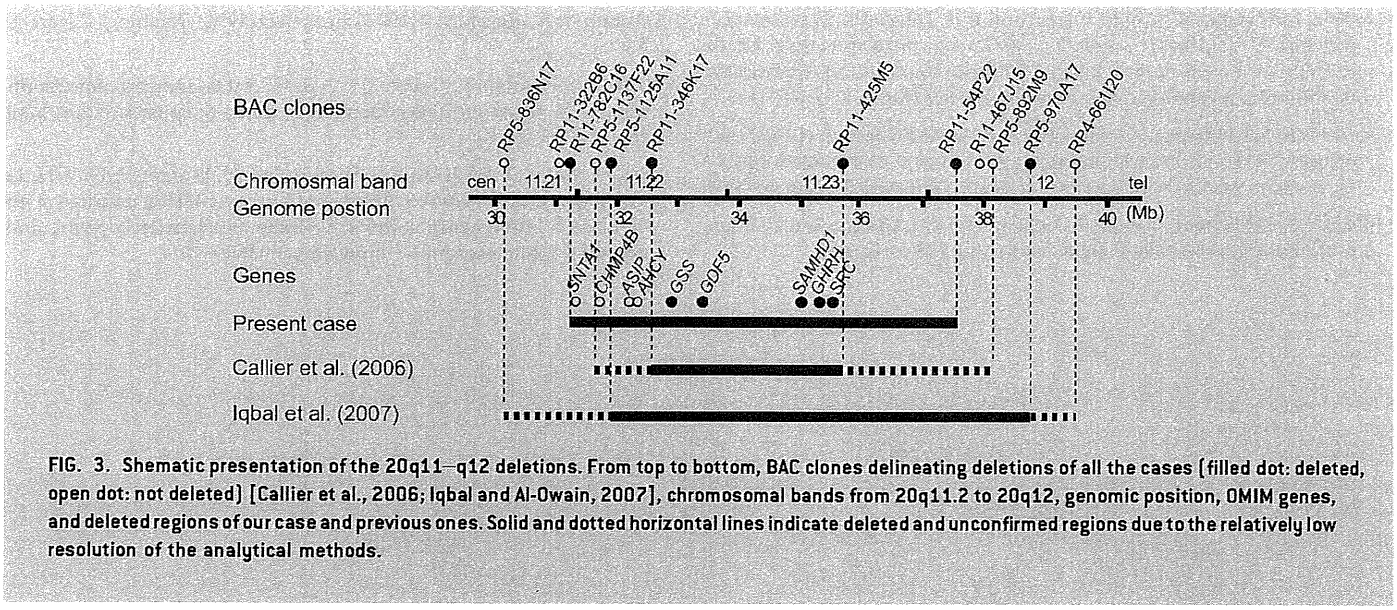

FIG. 3. Shematic presentation of the 20q11–q12 deletions. From top to bottom, BAC clones delineating deletions of all the cases [filled dot: deleted, open dot: not deleted] [Callier et al., 2006; Iqbal and Al-Owain, 2007], chromosomal bands from 20q11.2 to 20q12, genomic position, OMIM genes, and deleted regions of our case and previous ones. Solid and dotted horizontal lines indicate deleted and unconfirmed regions due to the relatively low resolution of the analytical methods.

OMIM #113100) by in vitro studies. As our patient has the *GDF5* haploinsufficiency, he may have the risk for BDC. However, he did not show this manifestation. He did have polydactyly, talipes valgus, and absence of the middle phalanges of the toes, which have been often found in individuals with BDC [Everman et al., 2002; Temtamy and Aglan, 2008]. Our patient did have a fetal akinesia (or hypokinesia) deformation phenotype (FADP). The short neck, hypertelorism, micrognathia, small thorax, postnatal respiratory disturbance, prolonged feeding difficulty, and slender long bone could represent FADP. FADP is a clinically and genetically heterogeneous constellation arising from fetal akinesia or decrease in utero movement due to intrinsic factors including neuropathy, myopathy, and restrictive dermopathy or extrinsic factors that limit fetal movement (e.g., tetragen exposure or fetal crowding) [Witters et al., 2002; Bamshad et al., 2009]. As extrinsic factors (e.g., abnormality of amniotic fluid, fetal crowding, congenital infection, and use of the drug in utero) could not be confirmed in this patient and the arthrogryposis and FADP are accompanied by other organ anomalies and developmental delay, the gene(s) at 20q11.21–q11.23 may be a primary intrinsic cause. Unfortunately, as skeletal malformations in the other two cases having the 20q11.2–q12 deletion were not fully described [Callier et al., 2006; Iqbal and Al-Owain, 2007], it is difficult to discuss the relationship between skeletal features and gene(s) in 20q11.2–q12 deletion.

Retinal dysplasia associated with falciform retinal fold and impaired vision was also noted. Retinal dysplasia is defined as abnormal growth and differentiation of embryonic retina either due to in utero environmental factors such as viral infection, tetragen exposure, retinopathy of prematurity or genetic factors. To our knowledge, this is the first description of retinal dysplasia associated with 20q11.2–q12 deletion.

ACKNOWLEDGMENTS

We are grateful to the patient and his family for their participation and support to this study. Grant-in Aid for Japan Society for the Promotion of Science (JSPS) Fellow (A.N.), Research Grants from the Ministry of Health, Labour and Welfare (N.M.), Grant-in-Aid from the Ministry of Education, Culture, Sports, Science and Technology of Japan (N.M.), and Grant-in-Aid for Scientific Research from JSPS (N.M.).

REFERENCES

Aldred MA, Aftimos S, Hall C, Waters KS, Thakker RV, Trembath RC, Brueton L. 2002. Constitutional deletion of chromosome 20q in two patients affected with albright hereditary osteodystrophy. Am J Med Genet 113:167–172.

Bamshad M, Van Heest AE, Pleasure D. 2009. Arthrogryposis: A review and update. J Bone Joint Surg Am 91:40–46.

Borozdin W, Graham JM Jr, Bohm D, Bamshad MJ, Spranger S, Burke L, Leipoldt M, Kohlhase J. 2007. Multigene deletions on chromosome 20q13.13-q13.2 including SALL4 result in an expanded phenotype of Okihiro syndrome plus developmental delay. Hum Mutat 28:830.

Callier P, Faivre L, Marle N, Thauvin-Robinet C, Sanlaville D, Gosset P, Prieur M, Labenne M, Huet F, Mugneret F. 2006. Major feeding difficulties in the first reported case of interstitial 20q11.22-q12 microdeletion and molecular cytogenetic characterization. Am J Med Genet Part A 140A:1859–1863.

Everman DB, Bartels CF, Yang Y, Yanamandra N, Goodman FR, Mendoza-Londono JR, Savarirayan R, White SM, Graham JM Jr, Gale RP, Svarch E, Newman WG, Kleckers AR, Francomano CA, Govindaiah V, Singh L, Morrison S, Thomas JT, Warman ML. 2002. The mutational spectrum of brachydactyly type C. Am J Med Genet 112:291–296.

Genevieve D, Sanlaville D, Faivre L, Kottler ML, Jambou M, Gosset P, Boustani-Samara D, Pinto G, Ozilou C, Abeguile G, Munnich A, Romana S, Raoul O, Cormier-Daire V, Vekemans M. 2005. Paternal deletion of the GNAS imprinted locus (including Gnasxl) in two girls presenting with severe pre- and post-natal growth retardation and intractable feeding difficulties. Eur J Hum Genet 13:1033–1039.

Iqbal MA, Al-Owain M. 2007. Interstitial del(20)(q11.2q12)—Clinical and molecular cytogenetic characterization. Am J Med Genet Part A 143A:1880–1884.

Kanda T, Murayama K, Kondo I, Kitazumi E, Takahashi K, Nakatani K, Yoneyama A, Yamori Y, Kanda Y. 2005. An estimation chart for the possibility of aspiration in patients with severe motor and intellectual disabilities: Its reliability and accuracy. No To Hattatsu 37:307–316.

Petersen MB, Tranebjaerg L, Tommerup N, Nygaard P, Edwards H. 1987. New assignment of the adenosine deaminase gene locus to chromosome 20q13 X 11 by study of a patient with interstitial deletion 20q. J Med Genet 24:93–96.

Shabtai F, Ben-Sasson E, Arieli S, Grinblat J. 1993. Chromosome 20 long arm deletion in an elderly malformed man. J Med Genet 30:171–173.

Temtamy SA, Aglan MS. 2008. Brachydactyly. Orphanet J Rare Dis 3:15.

Witters I, Moerman P, Fryns JP. 2002. Fetal akinesia deformation sequence: A study of 30 consecutive in utero diagnoses. Am J Med Genet 113:23–28.

Yang W, Cao L, Liu W, Jiang L, Sun M, Zhang D, Wang S, Lo WH, Luo Y, Zhang X. 2008. Novel point mutations in GDF5 associated with two distinct limb malformations in Chinese: Brachydactyly type C and proximal symphalangism. J Hum Genet 53:368–374.

REPORT

Mutations in *POLR3A* and *POLR3B* Encoding RNA Polymerase III Subunits Cause an Autosomal-Recessive Hypomyelinating Leukoencephalopathy

Hirotomo Saitsu,[1,*] Hitoshi Osaka,[2] Masayuki Sasaki,[3] Jun-ichi Takanashi,[4] Keisuke Hamada,[5] Akio Yamashita,[6] Hidehiro Shibayama,[7] Masaaki Shiina,[5] Yukiko Kondo,[1] Kiyomi Nishiyama,[1] Yoshinori Tsurusaki,[1] Noriko Miyake,[1] Hiroshi Doi,[1] Kazuhiro Ogata,[5] Ken Inoue,[8] and Naomichi Matsumoto[1,*]

Congenital hypomyelinating disorders are a heterogeneous group of inherited leukoencephalopathies characterized by abnormal myelin formation. We have recently reported a hypomyelinating syndrome characterized by diffuse cerebral hypomyelination with cerebellar atrophy and hypoplasia of the corpus callosum (HCAHC). We performed whole-exome sequencing of three unrelated individuals with HCAHC and identified compound heterozygous mutations in *POLR3B* in two individuals. The mutations include a nonsense mutation, a splice-site mutation, and two missense mutations at evolutionally conserved amino acids. Using reverse transcription-PCR and sequencing, we demonstrated that the splice-site mutation caused deletion of exon 18 from *POLR3B* mRNA and that the transcript harboring the nonsense mutation underwent nonsense-mediated mRNA decay. We also identified compound heterozygous missense mutations in *POLR3A* in the remaining individual. *POLR3A* and *POLR3B* encode the largest and second largest subunits of RNA Polymerase III (Pol III), RPC1 and RPC2, respectively. RPC1 and RPC2 together form the active center of the polymerase and contribute to the catalytic activity of the polymerase. Pol III is involved in the transcription of small noncoding RNAs, such as 5S ribosomal RNA and all transfer RNAs (tRNA). We hypothesize that perturbation of Pol III target transcription, especially of tRNAs, could be a common pathological mechanism underlying *POLR3A* and *POLR3B* mutations.

Congenital hypomyelinating disorders form a heterogeneous group of central nervous system leukoencephalopathies that is characterized by abnormal myelin formation. Although these conditions are readily recognized by brain magnetic resonance imaging (MRI), many cases are not diagnosed correctly.[1] Several syndromes affecting myelination, such as hypomyelination with hypodontia and hypogonadotropic hypogonadism (4H) syndrome (MIM 612440) and hypomyelination with atrophy of the basal ganglia and cerebellum (H-ABC) (MIM 612438), have been described.[2–5] We have recently reported a hypomyelinating syndrome characterized by diffuse cerebral hypomyelination with cerebellar atrophy and hypoplasia of the corpus callosum (HCAHC).[6] Individuals with HCAHC do not show hypodontia or atrophy of the basal ganglia, which are observed in 4H syndrome and H-ABC; however, diffuse hypomyelination, atrophy, or hypoplasia of the cerebellum and corpus callosum are overlapping features of these three syndromes, suggesting that there might be a common underlying pathological mechanism.

Here, we report on four individuals with HCAHC from three unrelated families (Figure 1A; Table 1). Clinical information and peripheral blood or saliva samples were obtained from the family members after obtaining written informed consent. Experimental protocols were approved by the Institutional Review Board of Yokohama City University. To identify pathogenic mutations, we performed whole-exome sequencing of three probands from three unrelated families (individuals 1, 3, and 4). DNAs were captured with the SureSelect Human All Exon 50Mb Kit (Agilent Technologies, Santa Clara, CA) and sequenced with one lane per sample on an Illumina GAIIx (Illumina, San Diego, CA) with 108 bp paired-end reads. Image analysis and base calling were performed by sequence control software real-time analysis and CASAVA software v1.7 (Illumina). A total of 90,014,368 (individual 1), 86,942,264 (individual 3), and 92,168,758 (individual 4) paired-end reads were obtained and aligned to the human reference genome sequence (GRCh37/hg19) with MAQ[7] and NextGENe software v2.00 with sequence condensation by consolidation (SoftGenetics, State College, PA). This approach resulted in more than 88% of target exomes being covered by ten reads or more (see Table S1, available online). Single nucleotide variants (SNVs) were called with MAQ and NextGENe. Small insertions and deletions were

[1]Department of Human Genetics, Yokohama City University Graduate School of Medicine, 3-9 Fukuura, Kanazawa-ku, Yokohama 236-0004, Japan; [2]Division of Neurology, Clinical Research Institute, Kanagawa Children's Medical Center, 2-138-4 Mutsukawa, Minami-ku, Yokohama 232-8555, Japan; [3]Department of Child Neurology, National Center of Neurology and Psychiatry, 4-1-1 Ogawahigashi-cho Kodaira, Tokyo 187-8551, Japan; [4]Department of Pediatrics, Kameda Medical Center, 929 Higashi-cho, Kamogawa-shi, Chiba 296-8602, Japan; [5]Department of Biochemistry, Yokohama City University Graduate School of Medicine, 3-9 Fukuura, Kanazawa-ku, Yokohama 236-0004, Japan; [6]Department of Molecular Biology, Yokohama City University Graduate School of Medicine, 3-9 Fukuura, Kanazawa-ku, Yokohama 236-0004, Japan; [7]Department of Neurology, Kameda Medical Center, 929 Higashi-cho, Kamogawa-shi, Chiba 296-8602, Japan; [8]Department of Mental Retardation and Birth Defect Research, National Institute of Neuroscience, National Center of Neurology and Psychiatry, 4-1-1 Ogawahigashi-cho Kodaira, Tokyo 187-8551, Japan
*Correspondence: hsaitsu@yokohama-cu.ac.jp (H.S.), naomat@yokohama-cu.ac.jp (N.M.)
DOI 10.1016/j.ajhg.2011.10.003.

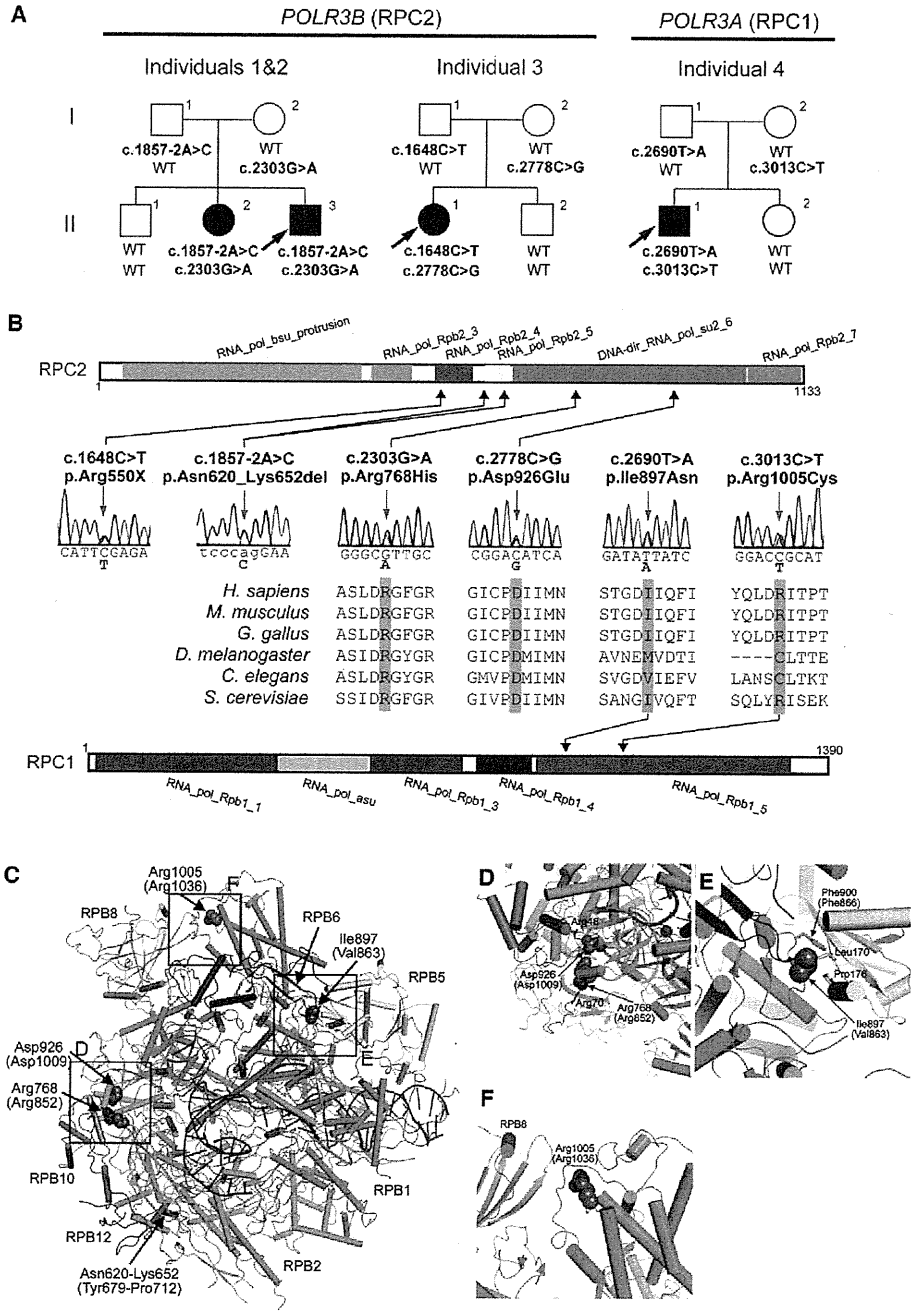

Figure 1. Mutations in *POLR3B* and *POLR3A*

(A) Pedigrees of four kindreds with HCAHC are shown. We identified four mutations in *POLR3B* encoding RPC2 in three individuals from two unrelated families and two mutations in *POLR3A* encoding RPC1 in one family. The segregation of each mutation is shown.

(B) Schematic representation of RPC2 (upper) and RPC1 (lower) proteins with Pfam domains (from Ensembl). Locations of each amino-acid-altering mutation are depicted with electropherograms. All of the missense mutations occurred at evolutionally conserved amino acids. Homologous sequences were aligned with the CLUSTALW website.

(C–F) 3D representations of RPC1 and RPC2 mutations. Mutated amino acids in RPC1 and RPC2 are shown along with their equivalent positions in the homologous RPB1 and RPB2 subunits of RNA Polymerase II (amino acid and its position in parenthesis). The structure and positions of mutations are illustrated by PyMOL with the crystal structure (PDB accession number 3GTP). RPB3, RPB9, and RPB11 subunits, which are specific to RNA Polymerase II, have been omitted from the figure. RPB1 is shown in green, RPB2 in sky blue, RPB5 in yellow, RPB6 in dark blue, RPB8 in pink, RPB10 in orange, RPB12 in purple, DNA in brown, and RNA in red. Amino acids that interact with mutated amino acids are also shown.

Table 1. Clinical Features of the Individuals

Clinical Features	Individual 1	Individual 2	Individual 3	Individual 4
Genes	*POLR3B*	*POLR3B*	*POLR3B*	*POLR3A*
Mutations, DNA	c.1857-2A>C, c.2303G>A	c.1857-2A>C, c.2303G>A	c.1648C>T, c.2778C>G	c.2690T>A, c.3013C>T
Mutations, protein	p.Asn620_Lys652del, p.Arg768His	p.Asn620_Lys652del, p.Arg768His	p.Arg550X, p.Asp926Glu	p.Ile897Asn, p.Arg1005Cys
Gender	M	F	F	M
Current age (years)	27	30	16	17
Intellectual disability	mild	mild	moderate	mild
Cognitive regression	–	–	–	–
Seizures	–	–	–	–
Initial motor development	normal	normal	normal	normal
Age of onset (years)	3	3	2	4
Motor deterioration	–	–	–	+
Wheelchair use	–	–	–	+
Optic atrophy	–	–	–	–
Myopia	+	+	–	+
Nystagmus	+	+	–	–
Abnormal pursuit	+	+	+	–
Vertical gaze limitation	+	+	+	–
Dysphagia	–	–	+	–
Hypersalivation	–	–	–	–
Cerebellar signs	+	+	+	+
Tremor	–	+	+	+
Babinski refex	–	–	–	–
Spasticity	–	–	mild	–
Peripheral nerve involvement	–	–	–	–
Nerve biopsy	NA	NA	NA	NA
Hypodontia	–	–	–	–
Hypogonadism	+	+	–	–

NA is an abbreviation for not available.

detected with NextGENe. Called SNVs were annotated with SeattleSeq Annotation.

We adopted a prioritization scheme to identify the pathogenic mutation in each individual, similar to the approach taken by recent studies (Table S2).[8–10] First, we excluded the variants registered in the dbSNP131 or 1000 Genome Project from all the detected variants. Then, SNVs commonly detected by MAQ and NextGENe analyses were selected as highly confident variants; 364 to 374 SNVs of nonsynonymous (NS) or canonical splice-site (SP) changes, along with 113 to 124 small insertions or deletions (indels), were identified per individual. We also excluded variants found in our 55 in-house exomes, which are derived from 12 healthy individuals and 43 individuals with unrelated diseases, reducing the number of candidate variants to ~250 per individual. Assuming that HCAHC is an autosomal-recessive disorder based on two affected individuals in one pedigree (individuals 1 and 2), we focused on rare heterozygous variants that are not registered in the dbSNP or in our in-house 55 exomes.

We surveyed all genes in each individual for two or more NS, SP, or indel variants. We found three to eight candidate genes per individual (Table S2). Among them, only *POLR3B* encoding RPC2, the second largest subunit of RNA Polymerase III (Pol III), was common in two individuals (individuals 1 and 3). The inheritance of the variants in *POLR3B* (transcript variant 1, NM_018082.5) was examined by Sanger sequencing. In individual 1, we confirmed that a canonical splice-site mutation (c.1857-2A>C [p.Asn620_Lys652del]), 2 bp upstream of exon 18, was

inherited from his father, and that a missense mutation (c.2303G>A [p.Arg768His]) in exon 21 were inherited from his mother (Figure 1A). The two mutations were also present in an affected elder sister (individual 2) but not present in a healthy elder brother. In individual 3, we confirmed that a nonsense mutation (c.1648C>T [p.Arg550X]) in exon 16 was inherited from her father and that a missense mutation (c.2778C>G [p.Asp926Glu]) in exon 24 was inherited from her mother (Figure 1A). The two mutations were not present in a healthy younger brother. To examine the mutational effects of c.1857-2A>C and c.1648C>T, reverse transcription PCR and sequencing with total RNA extracted from lymphoblastoid cells derived from the individuals was performed as previously described.[11] We demonstrated that the c.1857-2A>C mutation caused deletion of exon 18 from the *POLR3B* mRNA (Figures 2A–2C), resulting in an in-frame 33 amino acid deletion (p.Asn620_Lys652del) from RPC2 (Figure 1B). In addition, the mutated transcript harboring the nonsense mutation (c.1648C>T) was found to be expressed at a much lower level compared with the wild-type transcript (Figure 2D). The expression level of the mutated transcript was increased after treatment with 30 μM cycloheximide (CHX),[11] which inhibits nonsense-mediated mRNA decay (NMD), indicating that the mutant transcript underwent NMD (Figure 2D). The two missense mutations (p.Arg768His and p.Asp926Glu) found in the three individuals occurred at evolutionary conserved amino acids (Figure 1B). Among the other candidate genes in individuals 1 and 3, *MSLN* (MIM 601051), encoding mesothelin isoform 1 preproprotein that is cleaved into megakaryocyte potentiating factor and mesothelin, is a potential candidate in the family of individual 1 as its homozygous variant segregated with the phenotype; however, it is expressed in epithelial mesotheliomas, and the mutation affects less conserved amino acid (Table S3). The other candidate genes' variants did not cosegregate with the phenotype. Thus, mutations in *POLR3B* are most likely to cause HCAHC in two families.

In individual 4, in whom no *POLR3B* mutations were found, there were six candidate genes for an autosomal-recessive model. Among them, *POLR3A* (MIM 614258, GenBank accession number NM_007055.3), harboring two missense mutations, appeared to be a primary candidate because it encodes the largest subunit of Pol III (RPC1) (Figure 1A and Table S2). By Sanger sequencing, we confirmed that a missense mutation (c.2690T>A [p.Ile897Asn]) in exon 20 was inherited from his father and that another missense mutation (c.3013C>T [p.Arg1005Cys]) in exon 23 was inherited from his mother (Figure 1A). The two mutations were not present in a healthy younger sister. The two missense mutations (p.Ile897Asn and p.Arg1005Cys) occurred at relatively conserved amino acids (Figure 1B). In total, we found four mutations in *POLR3B* and two mutations in *POLR3A*. Evaluation of the missense mutations by PolyPhen-2 program showed that three mutations (p.Arg768His,

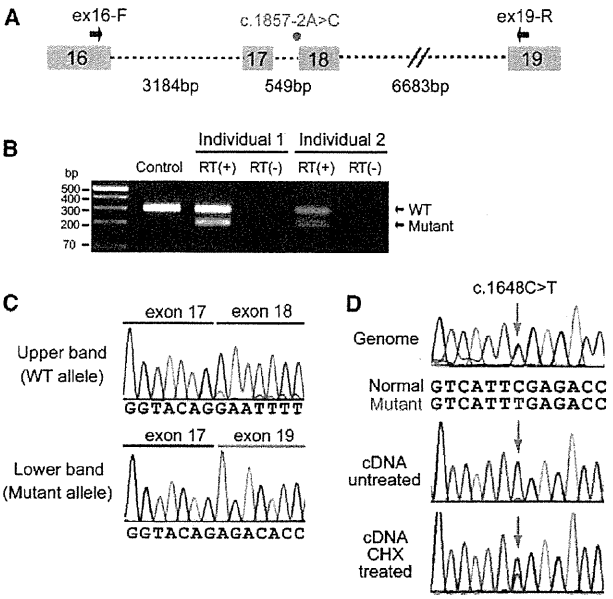

Figure 2. Effects of Splice-Site and Nonsense Mutations in *POLR3B*

(A) Schematic representation of the genomic structure of *POLR3B* from exon 16 to 19. Exons, introns, and primers are shown by boxes, dashed lines, and arrows, respectively. The mutation in intron 17 is depicted as a red dot.

(B) RT-PCR analysis of individuals 1 and 2 with c.1857-2A>C and a normal control. Two PCR products were detected from the individual's cDNA: the upper band is the wild-type (WT) transcript, and the lower band is the mutant. Only a single wild-type amplicon was detected in the control.

(C) Sequence of WT and mutant amplicons clearly showed exon 18 skipping in the mutant allele.

(D) Analysis of the c.1648C>T mutation. Sequence of PCR products amplified with genomic (upper), cDNA from untreated cells (middle), and cDNA from CHX treated cells (lower) as a template. Although untreated cells show extremely low levels of c.1648C>T mutant allele expression, cells treated to inhibit NMD show significantly increased levels of mutant allele expression.

p.Asp926Glu, and p.Ile897Asn) were probably damaging and that p.Arg1005Cys is tolerable. The c.2303G>A mutation (*POLR3B*) was found in one allele out of 540 Japanese control chromosomes. The remaining five mutations were not detected in 540 Japanese control chromosomes, indicating that the mutations are very rare in the Japanese population. Among the other candidate genes in individuals 4, *IGSF10*, a member of immunoglobulin superfamily, is a potential candidate because its variants segregated with the phenotype (Table S3); however, considering a close relationship between *POLR3A* and *POLR3B*, and the fact that *POLR3A* mutations have been recently reported in hypomyelinating leukodystrophy (see below),[12] *POLR3A* abnormality is the most plausible culprit for HCAHC in individual 4.

The structure of Pol III[13,14] and Pol II[15,16] is highly homologous, especially in the largest subunits. Thus, we extrapolated the mutations of RPC1 or RPC2 onto the structure of yeast Pol II (Protein Data Bank [PDB] accession number 3GTP)[17] (Figure 1C). RPB1 and RPB2 subunits of

yeast Pol II are homologous to RPC1 and RPC2 of Pol III, respectively. Asn620_Lys652 in RPC2 corresponds to Tyr679_Lys712 in RPB2. The deletion of Asn620_Lys652 (Tyr679_Lys712) would destroy a structural core of RPB2, leading to loss of RPB2 function. In addition, Arg768 (Arg852 in RPB2) interacts with the main-chain carbonyl group of Arg70 of the RPB12 subunit, and Asp926 (Asp1009 in RPB2) interacts with the side chain of Arg48 of the RPB10 subunit of Pol II (Figure 1D). Arg768His (Arg852His) and Asp926Glu (Asp1009Glu) substitutions are considered to disturb these subunit interactions, leading to dysfunction of the polymerase. Therefore, structural prediction suggests that the mutations in *POLR3B* (RPC2) could affect Pol III function. On the other hand, Ile897 and Arg1005 in RPC1 correspond to Val863 and Arg1036 in RPB1, respectively. Ile897 (Val863) has hydrophobic interactions with Leu170 and Pro176 of the RPB5 subunit and with Phe900 (Phe866) of the RPB1 subunit of Pol II (Figure 1E). Ile897Asn (Val863Asn) substitution is likely to disturb this interaction. Arg1005 (Arg1036) stabilizes interaction between RPB1 and RPB8 subunits (Figure 1F). The Arg1005Cys (Arg1036Cys) substitution appears to make this interaction unstable. Thus mutations in *POLR3A* are also predicted to affect Pol III function.

Clinical features of individuals with *POLR3A* or *POLR3B* mutations are presented in Table 1. MRI revealed high-intensity areas in the white matter in T2-weighted images, cerebellar atrophy, and a hypoplastic corpus callosum in all four individuals (Figure 3). Individuals 1 and 2 showed an extremely similar clinical course. They developed normally during their early infancy, i.e., walking unaided at 15 and 14 months, and uttering a few words at 12 and 13 months, respectively. After the age of 3, individual 1 presented with unstable walking and frequent stumbling and falling down, and individual 2 became poor at exercise. They both had severe myopia (corrected visual acuity of 0.7 and 0.5 at most, respectively). They graduated from elementary, junior high, and high schools with poor records, and the intelligence quotient (IQ) of individual 2 was 52 (WAIS-III). In individual 1, unstable walking was prominent at around 18 years, and he could not ride a bicycle because of ataxia; however, he could drive an automobile. Amenorrhea was noted in individual 2, and was successfully treated by hormone therapy. Individual 1 showed several signs of hypogonadism, including absence of underarm and mustache hair, thin pubic hair (Tanner II), and serum levels of testosterone, follicle stimulating hormone, and luteinizing hormone that were below normal for age 27. Neurological examination of both individuals revealed mild horizontal nystagmus, slowing of smooth-pursuit eye movement, and gaze limitation, especially in vertical gazing, hypotonia, mildly exaggerated deep-tendon reflex (patellar and Achilles tendon reflex) with negative Babinski reflex, and cerebellar signs and symptoms, including ataxic speech, wide-based ataxic gait, dysdiadochokinesis, and dysmetria. Clinical information for individual 3 has been reported previously.[6] Additional findings are as follows: slowing of smooth-pursuit eye movement, gaze limitation in vertical gazing, normal auditory brain responses (ABR), cerebral symptoms with mild spasticity, and intellectual disability (an IQ of 43 according to the WISC-III test), and no myopia but hypermetropic astigmatism. She showed no deterioration besides a mild dysphagia and walks herself to a school for the disabled. Individual 4 developed normally during his

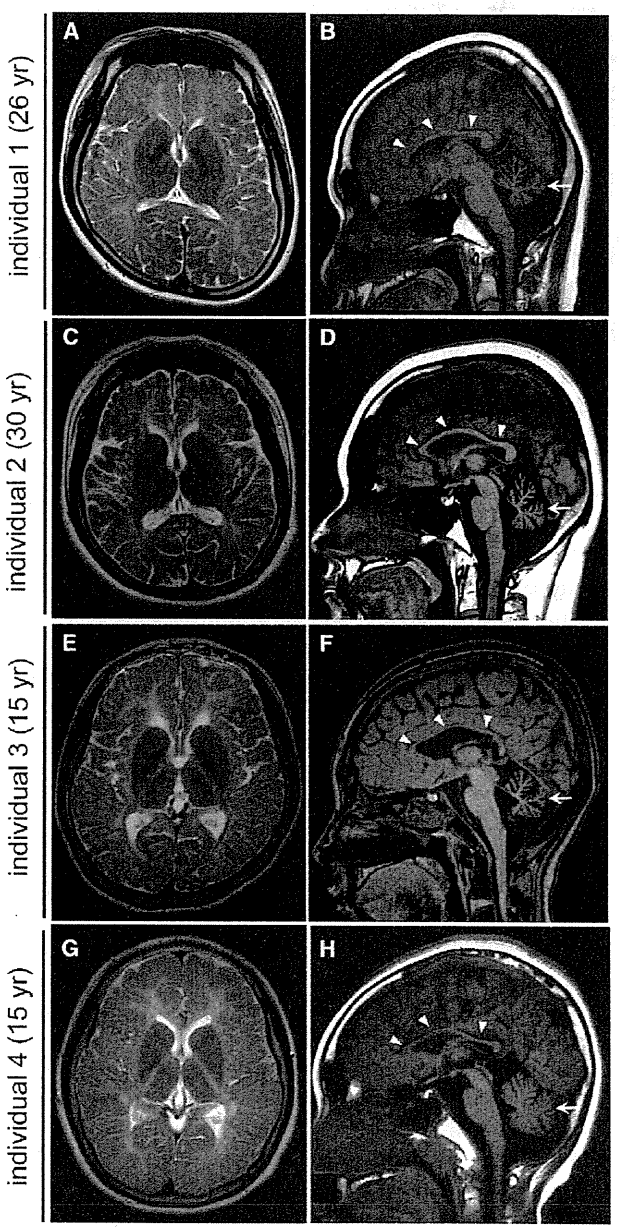

Figure 3. Brain MRI of Individuals with *POLR3B* and *POLR3A* Mutations

(A, C, E, and G) T2-weighted axial images through the basal ganglia. High-intensity areas in the white matter were observed in all individuals.

(B, D, F, and H) T1-weighted midline sagittal images. All the individuals showed hypoplastic corpus callosum (arrowheads) and atrophy of cerebellum (arrows).

early infancy, had normal head control at 3 months, was speaking a few words at 12 months, and was walking unaided at 14 months. His parents noted mild tremors around 4 years. He had normal stature, weight, and head circumference. Although he had severe myopia, his eye movement was smooth with no limitation or nystagmus. He had sensory neuronal deafness on the left side. He showed normal muscle tone and had no spasticity or rigidity. His tendon reflexes were slightly elevated with a negative Babinski reflex. Cerebellar signs were noted; expressive ataxic explosive speech, intension tremor, poor finger to nose test, dysdiadochokinesis, dysmetria, and wide-based ataxic gait. His intelligence quotient was 57 (according to the WISC-III test). His peripheral nerve conduction velocity was within the normal range and his ABR showed normal responses on the right side. He suffered motor deterioration around age 14 and became wheelchair bound.

In this study, we successfully identified compound heterozygous mutations in *POLR3A* and *POLR3B* in individuals with HCAHC. Very recently, Bernard et al.[12] reported that *POLR3A* mutations cause three overlapping leukodystrophies, including 4H syndrome, suggesting that HCAHC is, at least in part, within a wide clinical spectrum caused by *POLR3A* mutations. The p.Arg1005Cys mutation was shared between individual 9 in their report and our individual 4. All 19 individuals with *POLR3A* mutations showed progressive upper motor neuron dysfunction and cognitive regression. In addition, individual 9 showed abnormal eye movement, hypodontia, and hypogonadism. None of these features were recognized in our individual 4; these differences further support phenotypic variability of *POLR3A* mutations.[12] Given the phenotypic similarities among 4H syndrome, HCAHC, and H-ABC, there is a possibility that H-ABC is also allelic and caused by recessive mutations in either *POLR3A* or *POLR3B*.

Pol III consists of 17 subunits and is involved in the transcription of small noncoding RNAs, such as 5S ribosomal RNA (rRNA), U6 small nuclear RNA (snRNA), 7SL RNA, RNase P, RNase MRP, short interspersed nuclear elements (SINEs), and all transfer RNAs (tRNAs). Pol III-transcribed genes are classified into three types based on promoter elements and transcription factors. 5S rRNA is a solo type I gene. Type II genes include tRNA, 7SL RNA, and SINEs. Type III genes include U6 snRNA, RNase P, and RNase MRP.[18–20] The Pol III system is important for cell growth in yeast, and its transcription is tightly regulated during the cell cycle.[20] In zebrafish, *polr3b* mutant larvae that have a deletion of 41 conserved amino acids (Δ239-279) from the Rpc2 protein showed a proliferation deficit in multiple tissues, including intestine, endocrine pancreas, liver, retina and terminal branchial arches.[21] In the mutants, the expression levels of tRNA were significantly reduced, whereas the level of 5S rRNA expression was not changed, suggesting that this *polr3b* mutation can differentially affect Pol III target promoters.[21] RPC2 contributes to the catalytic activity of the polymerase and forms the active center of the polymerase together with the largest subunit, RPC1.[22] Thus, it is reasonable to consider that mutations in *POLR3A* and *POLR3B* cause overlapping phenotypes. Indeed, three individuals with *POLR3B* mutations showed diffuse cerebral hypomyelination, atrophy of the cerebellum and corpus callosum, and abnormal eye movements that overlap with *POLR3A* abnormalities.[12] Furthermore, two out of three individuals showed hypogonadism, suggesting a common pathological mechanism between *POLR3A* and *POLR3B* mutations. In the zebrafish *polr3b* mutants there were no defects of the central nervous system other than a reduced size of the retina, probably reflecting species differences; however, the reduced level of tRNA in the *polr3b* mutants raises the possibility that defects of tRNA transcription by Pol III could be a common pathological mechanism underlying *POLR3A* and *POLR3B* mutations. Supporting this idea, mutations in two genes involved in aminoacylation activity of tRNA synthetase cause defects of myelination in central nervous system: *DARS2* (MIM 610956) and *AIMP* (MIM 603605).[23,24] In addition, mutations in four genes encoding aminoacyl-tRNA synthetase cause Charcot-Marie-Tooth disease (MIM 613641, 613287, 601472, and 608323), resulting from demyelination of peripheral nerve axons: *KARS* (MIM 601421), *GARS* (MIM 600287), *YARS* (MIM 603623), and *AARS* (MIM 601065).[25–28] Thus, it is very likely that regulation of tRNA expression is essential for development and maintenance of myelination in both central and peripheral nervous systems.

An interesting clinical feature of *POLR3B* mutations is the absence of motor deterioration. All three individuals with *POLR3B* mutations could walk without support at ages 16, 27, and 30, whereas individual 3 with *POLR3A* mutations had motor deterioration around age 14. Bernard et al.[12] also reported progressive upper motor neuron dysfunction and cognitive regression in individuals with *POLR3A* mutations. Thus, there is a possibility that phenotypes caused by *POLR3A* mutations could be more severe and progressive than *POLR3B* mutant phenotypes. Identification of a greater number of cases with *POLR3B* mutations is required to confirm this hypothesis.

In conclusion, our data, together with that of a previous report,[12] demonstrate that mutations in Pol III subunits cause overlapping autosomal-recessive hypomyelinating disorders. Establishment of an animal model will facilitate our understanding of the pathophysiology of the multiple defects caused by Pol III mutations.

Supplemental Data

Supplemental Data include three tables and can be found with this article online at http://www.cell.com/AJHG/.

Acknowledgments

We would like to thank all the individuals and their families for their participation in this study. This work was supported by

research grants from the Ministry of Health, Labour, and Welfare (H.S., H.O., M.S., J.T., N. Miyake, K.I. and N. Matsumoto), the Japan Science and Technology Agency (N. Matsumoto), a Grant-in-Aid for Scientific Research on Innovative Areas (Foundation of Synapse and Neurocircuit Pathology) from the Ministry of Education, Culture, Sports, Science and Technology of Japan (N. Matsumoto), a Grant-in-Aid for Scientific Research from Japan Society for the Promotion of Science (H.O., N. Matsumoto), a Grant-in-Aid for Young Scientist from Japan Society for the Promotion of Science (H.S.). This work has been done at Advanced Medical Research Center, Yokohama City University.

Received: August 31, 2011
Revised: October 5, 2011
Accepted: October 10, 2011
Published online: October 27, 2011

Web Resources

The URLs for data presented herein are as follows:

ClustalW, http://www.genome.jp/tools/clustalw/
dbSNP, http://www.ncbi.nlm.nih.gov/projects/SNP/
Ensembl, http://uswest.ensembl.org/index.html
GenBank, http://www.ncbi.nlm.nih.gov/Genbank/
Online Mendelian Inheritance in Man, http://www.omim.org
PolyPhen-2, http://genetics.bwh.harvard.edu/pph2/
Protein Data Bank, http://www.pdb.org/pdb/home/home.do
PyMOL, http://www.pymol.org/
SeattleSeq Annotation, http://gvs.gs.washington.edu/SeattleSeq Annotation/

References

1. Schiffmann, R., and van der Knaap, M.S. (2009). Invited article: an MRI-based approach to the diagnosis of white matter disorders. Neurology *72*, 750–759.
2. Timmons, M., Tsokos, M., Asab, M.A., Seminara, S.B., Zirzow, G.C., Kaneski, C.R., Heiss, J.D., van der Knaap, M.S., Vanier, M.T., Schiffmann, R., and Wong, K. (2006). Peripheral and central hypomyelination with hypogonadotropic hypogonadism and hypodontia. Neurology *67*, 2066–2069.
3. Wolf, N.I., Harting, I., Boltshauser, E., Wiegand, G., Koch, M.J., Schmitt-Mechelke, T., Martin, E., Zschocke, J., Uhlenberg, B., Hoffmann, G.F., et al. (2005). Leukoencephalopathy with ataxia, hypodontia, and hypomyelination. Neurology *64*, 1461–1464.
4. Wolf, N.I., Harting, I., Innes, A.M., Patzer, S., Zeitler, P., Schneider, A., Wolff, A., Baier, K., Zschocke, J., Ebinger, F., et al. (2007). Ataxia, delayed dentition and hypomyelination: a novel leukoencephalopathy. Neuropediatrics *38*, 64–70.
5. van der Knaap, M.S., Naidu, S., Pouwels, P.J., Bonavita, S., van Coster, R., Lagae, L., Sperner, J., Surtees, R., Schiffmann, R., and Valk, J. (2002). New syndrome characterized by hypomyelination with atrophy of the basal ganglia and cerebellum. AJNR Am. J. Neuroradiol. *23*, 1466–1474.
6. Sasaki, M., Takanashi, J., Tada, H., Sakuma, H., Furushima, W., and Sato, N. (2009). Diffuse cerebral hypomyelination with cerebellar atrophy and hypoplasia of the corpus callosum. Brain Dev. *31*, 582–587.
7. Li, H., Ruan, J., and Durbin, R. (2008). Mapping short DNA sequencing reads and calling variants using mapping quality scores. Genome Res. *18*, 1851–1858.
8. Doi, H., Yoshida, K., Yasuda, T., Fukuda, M., Fukuda, Y., Morita, H., Ikeda, S., Kato, R., Tsurusaki, Y., Miyake, N., et al. (2011). Exome sequencing reveals a homozygous *SYT14* mutation in adult-onset, autosomal-recessive spinocerebellar ataxia with psychomotor retardation. Am. J. Hum. Genet. *89*, 320–327.
9. Pierce, S.B., Walsh, T., Chisholm, K.M., Lee, M.K., Thornton, A.M., Fiumara, A., Opitz, J.M., Levy-Lahad, E., Klevit, R.E., and King, M.C. (2010). Mutations in the DBP-deficiency protein HSD17B4 cause ovarian dysgenesis, hearing loss, and ataxia of Perrault Syndrome. Am. J. Hum. Genet. *87*, 282–288.
10. Gilissen, C., Arts, H.H., Hoischen, A., Spruijt, L., Mans, D.A., Arts, P., van Lier, B., Steehouwer, M., van Reeuwijk, J., Kant, S.G., et al. (2010). Exome sequencing identifies *WDR35* variants involved in Sensenbrenner syndrome. Am. J. Hum. Genet. *87*, 418–423.
11. Saitsu, H., Kato, M., Okada, I., Orii, K.E., Higuchi, T., Hoshino, H., Kubota, M., Arai, H., Tagawa, T., Kimura, S., et al. (2010). *STXBP1* mutations in early infantile epileptic encephalopathy with suppression-burst pattern. Epilepsia *51*, 2397–2405.
12. Bernard, G., Chouery, E., Putorti, M.L., Tetreault, M., Takanohashi, A., Carosso, G., Clement, I., Boespflug-Tanguy, O., Rodriguez, D., Delague, V., et al. (2011). Mutations of *POLR3A* Encoding a Catalytic Subunit of RNA Polymerase Pol III Cause a Recessive Hypomyelinating Leukodystrophy. Am. J. Hum. Genet. *89*, 415–423.
13. Jasiak, A.J., Armache, K.J., Martens, B., Jansen, R.P., and Cramer, P. (2006). Structural biology of RNA polymerase III: subcomplex C17/25 X-ray structure and 11 subunit enzyme model. Mol. Cell *23*, 71–81.
14. Fernández-Tornero, C., Böttcher, B., Riva, M., Carles, C., Steuerwald, U., Ruigrok, R.W., Sentenac, A., Müller, C.W., and Schoehn, G. (2007). Insights into transcription initiation and termination from the electron microscopy structure of yeast RNA polymerase III. Mol. Cell *25*, 813–823.
15. Cramer, P., Bushnell, D.A., and Kornberg, R.D. (2001). Structural basis of transcription: RNA polymerase II at 2.8 angstrom resolution. Science *292*, 1863–1876.
16. Gnatt, A.L., Cramer, P., Fu, J., Bushnell, D.A., and Kornberg, R.D. (2001). Structural basis of transcription: an RNA polymerase II elongation complex at 3.3 A resolution. Science *292*, 1876–1882.
17. Wang, D., Bushnell, D.A., Huang, X., Westover, K.D., Levitt, M., and Kornberg, R.D. (2009). Structural basis of transcription: backtracked RNA polymerase II at 3.4 angstrom resolution. Science *324*, 1203–1206.
18. Oler, A.J., Alla, R.K., Roberts, D.N., Wong, A., Hollenhorst, P.C., Chandler, K.J., Cassiday, P.A., Nelson, C.A., Hagedorn, C.H., Graves, B.J., and Cairns, B.R. (2010). Human RNA polymerase III transcriptomes and relationships to Pol II promoter chromatin and enhancer-binding factors. Nat. Struct. Mol. Biol. *17*, 620–628.
19. Dieci, G., Fiorino, G., Castelnuovo, M., Teichmann, M., and Pagano, A. (2007). The expanding RNA polymerase III transcriptome. Trends Genet. *23*, 614–622.
20. Dumay-Odelot, H., Durrieu-Gaillard, S., Da Silva, D., Roeder, R.G., and Teichmann, M. (2010). Cell growth- and differentiation-dependent regulation of RNA polymerase III transcription. Cell Cycle *9*, 3687–3699.

21. Yee, N.S., Gong, W., Huang, Y., Lorent, K., Dolan, A.C., Maraia, R.J., and Pack, M. (2007). Mutation of RNA Pol III subunit *rpc2/polr3b* Leads to Deficiency of Subunit Rpc11 and disrupts zebrafish digestive development. PLoS Biol. *5*, e312.
22. Werner, M., Thuriaux, P., and Soutourina, J. (2009). Structure-function analysis of RNA polymerases I and III. Curr. Opin. Struct. Biol. *19*, 740–745.
23. Scheper, G.C., van der Klok, T., van Andel, R.J., van Berkel, C.G., Sissler, M., Smet, J., Muravina, T.I., Serkov, S.V., Uziel, G., Bugiani, M., et al. (2007). Mitochondrial aspartyl-tRNA synthetase deficiency causes leukoencephalopathy with brain stem and spinal cord involvement and lactate elevation. Nat. Genet. *39*, 534–539.
24. Feinstein, M., Markus, B., Noyman, I., Shalev, H., Flusser, H., Shelef, I., Liani-Leibson, K., Shorer, Z., Cohen, I., Khateeb, S., et al. (2010). Pelizaeus-Merzbacher-like disease caused by AIMP1/p43 homozygous mutation. Am. J. Hum. Genet. *87*, 820–828.
25. Latour, P., Thauvin-Robinet, C., Baudelet-Méry, C., Soichot, P., Cusin, V., Faivre, L., Locatelli, M.C., Mayençon, M., Sarcey, A., Broussolle, E., et al. (2010). A major determinant for binding and aminoacylation of tRNA(Ala) in cytoplasmic Alanyl-tRNA synthetase is mutated in dominant axonal Charcot-Marie-Tooth disease. Am. J. Hum. Genet. *86*, 77–82.
26. McLaughlin, H.M., Sakaguchi, R., Liu, C., Igarashi, T., Pehlivan, D., Chu, K., Iyer, R., Cruz, P., Cherukuri, P.F., Hansen, N.F., et al. (2010). Compound heterozygosity for loss-of-function lysyl-tRNA synthetase mutations in a patient with peripheral neuropathy. Am. J. Hum. Genet. *87*, 560–566.
27. Antonellis, A., Ellsworth, R.E., Sambuughin, N., Puls, I., Abel, A., Lee-Lin, S.Q., Jordanova, A., Kremensky, I., Christodoulou, K., Middleton, L.T., et al. (2003). Glycyl tRNA synthetase mutations in Charcot-Marie-Tooth disease type 2D and distal spinal muscular atrophy type V. Am. J. Hum. Genet. *72*, 1293–1299.
28. Jordanova, A., Irobi, J., Thomas, F.P., Van Dijck, P., Meerschaert, K., Dewil, M., Dierick, I., Jacobs, A., De Vriendt, E., Guergueltcheva, V., et al. (2006). Disrupted function and axonal distribution of mutant tyrosyl-tRNA synthetase in dominant intermediate Charcot-Marie-Tooth neuropathy. Nat. Genet. *38*, 197–202.

CLINICAL GENETICS An International Journal of Genetics, Molecular and Personalized Medicine

Clin Genet 2011: 80: 293–296
Printed in Singapore. All rights reserved

CLINICAL GENETICS
doi: 10.1111/j.1399-0004.2011.01644.x

Letter to the Editor

A novel homozygous mutation of *DARS2* may cause a severe LBSL variant

To the Editor:

Leukoencephalopathy with brain stem and spinal cord involvement, and lactate elevation (LBSL, MIM #611105) is an autosomal recessive disorder with an early childhood-to-adolescence onset. In 2003, van der Knaap et al. originally described LBSL, which is characterized by slowly progressive pyramidal, cerebellar, and dorsal column dysfunction with increased white matter lactate levels in magnetic resonance (MR) spectroscopy (1). Since the first discovery that LBSL is caused by mutations of the *DARS2* gene-encoding mitochondrial aspartyl-tRNA synthetase (MtAspRS) (2), *DARS2* mutations have been found in all the patients described (2–5), but none of them showed a homozygous mutation (all are compound heterozygotes), suggesting that the activity of mutant MtAspRS homodimers may be incompatible with human life (2, 5). Here, we describe, for the first time, a consanguineous family with a homozygous *DARS2* mutation.

Materials and methods

We analyzed a consanguineous family including three affected children diagnosed with leukoencephalopathy (Fig. 1a and Table 1). The proband (II-2) developed truncal ataxic gait at 3 years old. Her affected sister (II-3) and brother (II-4) also showed truncal ataxia at 6 and 11 months, respectively. All cases were presented with horizontal nystagmus, slurring speech, ataxic gait, muscle tonus abnormality, hypo- or hyperreflexia, and tremor as well as mental retardation. II-2 at age 21 years could slowly speak one or two words. Peripheral muscles atrophy, weakness and joints contractures in extremities, loss of deep tendons reflex and disturbed deep sensation were noted. II-3 and II-4 died of pneumonia at age 8 years and respiratory failure at age 2 years, respectively. Although there were differences in MR imaging characteristics from classical LBSL, there were also striking similarities. In our patients, the involvement of the cerebral and cerebellar white matter was more diffused and severe than in classical LBSL, but the affected brain stem and spinal cord tracts were the same (Fig. 1b and Table 1).

Linkage analysis and direct sequencing of *DARS2* were performed as previously reported (6). Immunoblotting was carried out using antihuman DARS2 antibody (ab69336, Abcam, Cambridge, UK) and anti-cytochrome *c* oxidase (COX) IV antibody (ab16056, Abcam).

Results

Homozygosity mapping of this consanguineous family revealed the largest 8.5 Mb homozygous region at chromosome 1q25.1 with the maximum LOD score of 1.329. Five additional microsatellite markers showed the consistent result (Fig. 1a). Within this region, *DARS2* gene was highlighted as the primary target as it was causative for the LBSL. We found that all affected children possessed homozygous, and parents and an unaffected sib had the heterozygous intronic change at 22 base pairs upstream of exon 3 (c.228-22T>A), respectively. This change was not observed in 395 controls. We examined its mutational effect by reverse transcriptase-polymerase chain reaction (RT-PCR) using mRNA of lymphoblastoid cell lines (LCLs) derived from the proband, her father (a carrier) and a normal control. A shorter PCR fragment which lacked the entire exon 3 was confirmed by sequencing (Fig. 1c,d). Furthermore, wild-type *DARS2* mRNA and MtAspRS protein were significantly decreased in proband's LCL (Fig. 1e,f). Other genes within the 1q25.1 region have not been checked.

Discussion

We found a novel homozygous mutation of *DARS2* in a diffuse leukoencephalopathy, which may be an LBSL variant. This change resulted in the decrease of normal protein level and may have contributed to this disease. Two possibilities for the increased severity are considered: (i) a

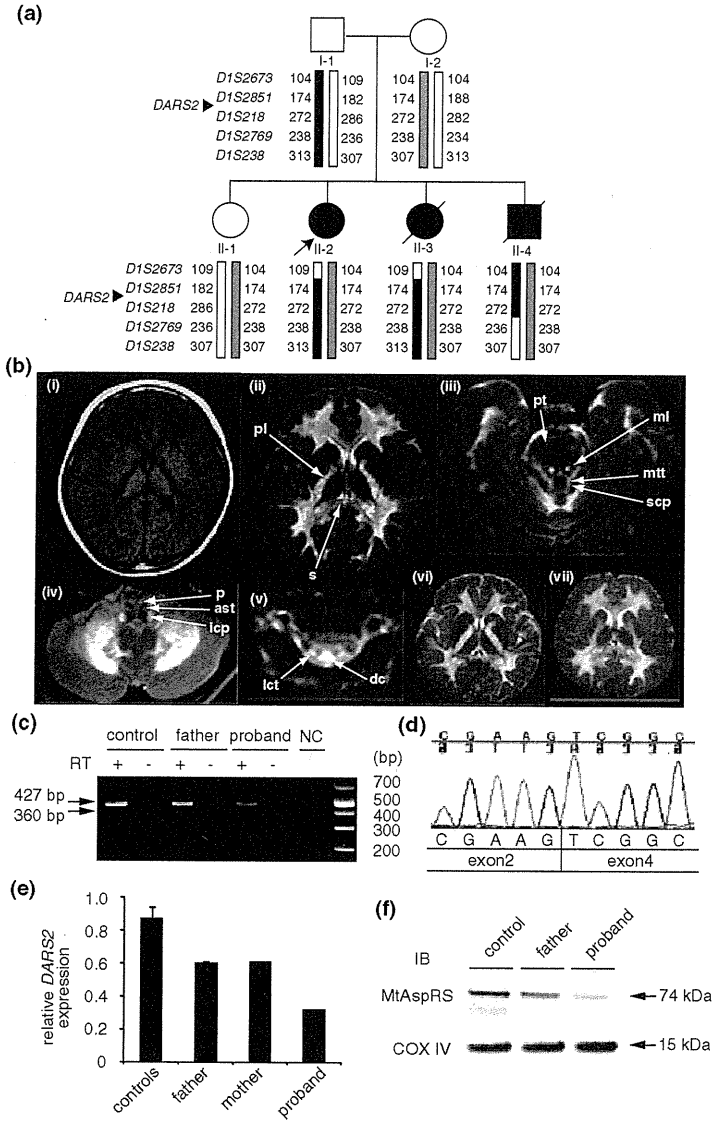

Fig. 1. Identification of a homozygous *DARS2* mutation causing abnormal splicing. (**a**) Haplotype analysis of the family. The black and gray bars represent disease alleles. The *DARS2* gene is located in between *D1S2851* and *D1S218*. (**b**) Magnetic resonance (MR) images of central nervous system in the proband (II-2) at 5 years (i–v), II-3 at 5 years (vi) and II-4 at 1 year and 4 months of age (vii). T_1-weighted (i) and T_2-weighted (T_2) (ii) images of cerebrum. The cerebral white matter was diffusely and severely affected, while the cerebral white matter involvement is less severe and more limited in extent in leukoencephalopathy with brain stem and spinal cord involvement, and lactate elevation with sparing of the U-fibers. Inhomogeneous signal abnormalities were observed in the posterior limb (pl) of the internal capsule and the splenium (s) of the corpus callosum. (iii) T_2 image at the level of the pons. The abnormal high-intensity signals were observed in pyramidal tracts (pt), medial lemniscus (ml), mesencephalic trigeminal tracts (mtt) and superior cerebellar peduncles (scp). (iv) T_2 image at the level of medulla. The pyramids (p), anterior spinocerebellar tracts (ast) and inferior cerebellar peduncles (icp) were affected. (v) T_2 image at the level of the cervical spinal cord. The dorsal columns (dc) and lateral corticospinal tracts (lct) showed abnormal signals. II-3 (vi) and II-4 (vii) showed the similar MR images as the proband. (**c**) RT-PCR using cDNA extracted from LCLs of a normal control, father and the proband. A shorter fragment (360 bp) in addition to a normal product (427 bp) was seen in father and the proband. (**d**) Electropherogram of the shorter fragment showing skipping of exon 3. (**e**) Relative expression of wild-type *DARS2* mRNA compared to β-actin mRNA in LCLs were determined by quantitative real-time RT-PCR using TaqMan Gene Expression Assays (Applied Biosystems, Bedford, MA). The relative *DARS2* expression was analyzed using TaqMan Probe (Applied Biosystems, Hs01016215_m1 for *DARS2* and 4326135E for β-actin as a control). Levels are shown for three controls, parents and the proband based on the calibration curve method using an independent control. Average of duplicated experiments is shown as black bars with the standard error of means. The significant decreased expression of *DARS2* mRNA in the proband was recognized compared to that in three controls ($p < 0.001$, one-way analysis of variance with Bonferroni's multiple comparison test). (**f**) Mitochondrial aspartyl-tRNA synthetase (MtAspRS) protein is expressed in normal control and father as a carrier (fainter), but only weakly recognized in the proband. Cyclooxygenase IV was used as a loading control for the mitochondrial fraction.

Table 1. MRI criteria for LBSL and clinical features of patients

Diagnostic criteria	Case 1	Case 2	Case 3
Major criteria			
Signal abnormalities in			
1. the cerebral white matter, either inhomogeneous and spotty or homogeneous and confluent, sparing the U-fibers	±[a]	±[a]	±[a]
2. the dorsal columns and lateral corticospinal tracts of the spinal cord. (visualization of such abnormalities in the cervical spinal cord suffices)	+	n.e.[b]	n.e.
3. the pyramids of the medulla oblongata	+	+	+
Supportive criteria			
Signal abnormalities in			
1. the splenium of the corpus callosum	+	+	+
2. the posterior limb of the internal capsule	+	+	+
3. the medial lemniscus in the brain stem	+	+	+
4. the superior cerebellar peduncles	+	+	+
5. the inferior cerebellar peduncles	+	n.e.	n.e.
6. the intraparenchymal part of the trigeminal nerve	−	n.e.	n.e.
7. the mesencephalic trigeminal tracts	+	n.e.	n.e.
8. the anterior spinocerebellar tracts in the medulla	+	n.e.	n.e.
9. the cerebellar white matter with subcortical preponderance	−	−	−
Elevated lactate of abnormal cerebral white matter (MRS)	+	Not performed	+

LBSL, leukoencephalopathy with brain stem and spinal cord involvement, and lactate elevation; MRI, magnetic resonance imaging; MRS, magnetic resonance spectroscopy.
[a]Homogeneous and confluent abnormal high intensity was observed, but sparing the U-fibers was unclear because of the strenuous pathological change in the white matter.
[b]n.e., not evaluated as MRI images were unavailable.

(unidentified) modifier effect in the family and (ii) this particular homozygous mutation caused the severe variant because of the substantially decreased normal protein level, although it is not full proof.

Interestingly, affected allele frequency varies, depending on the ethnicity. For example, *DARS2* mutations are the most common causes of childhood onset leukoencephalopathy in Finland, because of high carrier frequency (1:95 for the c.228-20_21delTTinsC and 1:380 for the c.492+2T>C) (4). Thus, further analysis of the *DARS2* gene in LBSL as well as childhood-to-adult onset leukoencephalopathy of unknown cause in different populations would lead us to fully understand phenotypes of the *DARS2* abnormalities.

Acknowledgements

We thank all the patients and their families for participating in this work. We also thank Ms. Y. Yamashita for her technical assistance. This work was supported by Research Grants from the Ministry of Health, Labour and Welfare (N. M., H. S., and N. M.), the Japan Science and Technology Agency (N. M.), Grant-in-Aid for Scientific Research from Japan Society for the Promotion of Science (N. M.), Grant-in-Aid for Young Scientist from Japan Society for the Promotion of Science (N. M. and H. S.), Grant for 2010 Strategic Research Promotion of Yokohama City University (N. M.), Research Grants from the Japan Epilepsy Research Foundation (H. S.), and Research Grant from Naito Foundation (N. M.), the Takeda Science Foundation (N. M. and N. M.), the Yokohama Foundation for Advancement of Medical Science (N. M.), and the Hayashi Memorial Foundation for Female Natural Scientists (N. M.).

N Miyake[a]
S Yamashita[b]
K Kurosawa[c]
S Miyatake[a]
Y Tsurusaki[a]
H Doi[a]
H Saitsu[a]
N Matsumoto[a]
[a]Department of Human Genetics, Yokohama City University Graduate School of Medicine, Yokohama, Japan,
[b]Division of Child Neurology, and
[c]Division of Medical Genetics, Kanagawa Children's Medical Center, Yokohama, Japan

References

1. van der Knaap MS, van der Voorn P, Barkhof F et al. A new leukoencephalopathy with brainstem and spinal cord involvement and high lactate. Ann Neurol 2003: 53: 252–258.
2. Scheper GC, van der Klok T, van Andel RJ et al. Mitochondrial aspartyl-tRNA synthetase deficiency causes leukoencephalopathy with brain stem and spinal cord involvement and lactate elevation. Nat Genet 2007: 39: 534–539.
3. Uluc K, Baskan O, Yildirim KA et al. Leukoencephalopathy with brain stem and spinal cord involvement and high lactate:

a genetically proven case with distinct MRI findings. J Neurol Sci 2008: 273: 118–122.
4. Isohanni P, Linnankivi T, Buzkova J et al. *DARS2* mutations in mitochondrial leucoencephalopathy and multiple sclerosis. J Med Genet 2010: 47: 66–70.
5. Lin J, Faria EC, Da Rocha AJ et al. Leukoencephalopathy with brainstem and spinal cord involvement and normal lactate: a new mutation in the *DARS2* gene. J Child Neurol 2010: 25: 1425–1428.
6. Miyake N, Kosho T, Mizumoto S et al. Loss-of-function mutations of *CHST14* in a new type of Ehlers-Danlos syndrome. Hum Mutat 2010: 31: 966–974.

Correspondence:
Noriko Miyake, MD, PhD
Department of Human Genetics
Yokohama City University Graduate School of Medicine
3-9 Fukuura
Kanazawa-ku
236-0004 Yokohama
Japan
Tel.: +81 45 787 2606
Fax: +81 45 786 5219
e-mail: nmiyake@yokohama-cu.ac.jp

CLINICAL REPORT

AMERICAN JOURNAL OF medical genetics PART A

Early Infantile Epileptic Encephalopathy Associated With the Disrupted Gene Encoding Slit-Robo Rho GTPase Activating Protein 2 (*SRGAP2*)

Hirotomo Saitsu,[1]* Hitoshi Osaka,[2] Shirou Sugiyama,[2] Kenji Kurosawa,[3] Takeshi Mizuguchi,[1] Kiyomi Nishiyama,[1] Akira Nishimura,[1] Yoshinori Tsurusaki,[1] Hiroshi Doi,[1] Noriko Miyake,[1] Naoki Harada,[4] Mitsuhiro Kato,[5] and Naomichi Matsumoto[1]

[1]Department of Human Genetics, Graduate School of Medicine, Yokohama City University, Kanazawa-ku, Yokohama, Japan

[2]Division of Neurology, Clinical Research Institute, Kanagawa Children's Medical Center, Minami-ku, Yokohama, Japan

[3]Division of Medical Genetics, Clinical Research Institute, Kanagawa Children's Medical Center, Minami-ku, Yokohama, Japan

[4]Cytogenetic Testing Group B, Advanced Medical Science Research Center, Mitsubishi Chemical Medience Corporation, Nagasaki, Japan

[5]Faculty of Medicine, Department of Pediatrics, Yamagata University Yamagata, Japan

Received 25 January 2011; Accepted 31 July 2011

We report on a female patient with early infantile epileptic encephalopathy and severe psychomotor disability possessing a de novo balanced translocation t(1;9)(q32;q13). The patient showed clonic convulsions of extremities 2 days after birth. Electroencephalogram (EEG) transiently showed atypical suppression-burst pattern. The seizures evolved to brief tonic spasms, and hypsarrhythmia on EEG was noticed at age of 5 months, indicating the transition to West syndrome. By using fluorescent in situ hybridization (FISH), southern hybridization, and inverse PCR, the translocation breakpoints were successfully determined at the nucleotide level. The 1q32.1 breakpoint was located within a segmental duplication and disrupted the gene encoding Slit-Robo Rho GTPase activating protein 2 (*SRGAP2*). The 9q13 breakpoint was suggested to reside in the heterochromatin region. *Srgap2* has been shown to be specifically expressed in developing brain of rodents, negatively regulate neuronal migration and induce neurite outgrowth and branching. Thus, *SRGAP2* is very likely to play a role in the developing human brain. This is a first report of the *SRGAP2* abnormality associated with early infantile epileptic encephalopathy.

Key words: early infantile epileptic encephalopathy; West syndrome; chromosomal translocation; *SRGAP2*

How to Cite this Article:
Saitsu H, Osaka H, Sugiyama S, Kurosawa K, Mizuguchi T, Nishiyama K, Nishimura A, Tsurusaki Y, Doi H, Miyake N, Harada N, Kato M, Matsumoto N. 2012. Early infantile epileptic encephalopathy associated with the disrupted gene encoding Slit-Robo Rho GTPase activating protein 2 (*SRGAP2*).
Am J Med Genet Part A 158A:199–205.

INTRODUCTION

Many infantile epileptic syndromes show a unique combination of seizure types and electroencephalogram (EEG) findings depending on the patients' age [Kato et al., 2008]. Ohtahara syndrome (OS) and early myoclonic encephalopathy (EME) are characterized by early onset seizures mainly in neonatal period, and suppression-burst pattern on EEG, though their initial seizure type is different [Djukic et al., 2006; Ohtahara and Yamatogi, 2006]. Both OS and EME can progress to the West syndrome phenotype age-dependently, which is characterized by brief tonic spasms, a specific EEG pattern called hypsarrhythmia [Kato, 2006], in 75% and 41% of cases, respectively [Djukic et al., 2006; Ohtahara and Yamatogi, 2006]. The three epileptic syndromes (OS, EME, and West syndrome) are generally intractable and show the arrest of psychomotor development [Djukic et al., 2006; Kato, 2006; Ohtahara and Yamatogi, 2006]. Brain malformations and metabolic disorders were found as underlying causes of the three syndromes, but

Grant sponsor: Ministry of Health, Labour and Welfare; Grant sponsor: Japan Society for the Promotion of Science; Grant sponsor: Yokohama Foundation for Advancement of Medical Science; Grant sponsor: Japan Epilepsy Research Foundation; Grant sponsor: Naito Foundation.
*Correspondence to:
Dr. Hirotomo Saitsu, Department of Human Genetics, Yokohama City University Graduate School of Medicine, Fukuura 3-9, Kanazawa-ku, Yokohama 236-0004, Japan. E-mail: hsaitsu@yokohama-cu.ac.jp
Published online 21 November 2011 in Wiley Online Library (wileyonlinelibrary.com).
DOI 10.1002/ajmg.a.34363

many idiopathic or cryptogenic cases remain etiologically unexplained. Recently, several causative genes have been reported: *ARX* in OS and West syndrome, *CDKL5* in West syndrome, *STXBP1* in OS, *SLC25A22* in EME [Stromme et al., 2002; Kalscheuer et al., 2003; Weaving et al., 2004; Molinari et al., 2005; Kato et al., 2007; Saitsu et al., 2008]. Of note, mutations in *ARX* have been found in both OS and West syndrome phenotypes, suggesting a common pathological seizure mechanism between them. However, there are still large numbers of cases remaining to be elucidated. Identification of new causative genes is absolutely necessary for further understanding of infantile epileptic syndromes.

The Slit-Robo signaling controls the neuronal migration and axonal guidance [Brose et al., 1999; Li et al., 1999; Wu et al., 1999], both of which are dependent on cytoskeletal reorganization. The family of Rho-GTPases, including Rac, Cdc42, and Rho, plays important roles in regulating cytoskeletal dynamics [Hall, 1998]. Rho-GTPases alternate between active (GTP-bound) and inactive (GDP-bound) conformation. The activities of Rho GTPases are tightly and antagonistically regulated by Guanine nucleotide exchange factors (GEFs) and GTPase activating proteins (GAPs): GEFs catalyze nucleotide exchange and mediate activation, while GAPs increase the intrinsic GTPase activities to promote GTP hydrolysis, leading to inactivation [Lamarche and Hall, 1994]. Slit-Robo Rho GTPase activating proteins (SRGAPs) were identified as a family of GAP proteins which bind to the intracellular domain of Robo [Wong et al., 2001]. Three family members (SRGAP1-3) specifically expressed in developing brain of rodents [Wong et al., 2001; Yao et al., 2008; Bacon et al., 2009]. Recent studies suggested that SRGAPs are involved in neuronal development. SRGAP1 protein is required for Slit-mediated repulsion of migratory cells from the anterior subventricular zone of the forebrain by blocking Cdc42 activity [Wong et al., 2001]. Functional disruption of SRGAP3 protein is associated with severe mental retardation in 3p-syndrome [Endris et al., 2002]. Moreover, it has been reported that SRGAP2 negatively regulates neuronal migration and induces neurite outgrowth and branching [Guerrier et al., 2009].

Here, we present a patient with infantile epileptic encephalopathy and profound psychomotor delay with a de novo reciprocal translocation t(1;9)(q32;q13), disrupting the *SRGAP2* gene. Detailed genomic analysis is presented.

CLINICAL REPORT

The 5-year-old girl is a product of unrelated healthy parents. She was born at term without asphyxia after an uneventful pregnancy. She showed apnea twice at day 1. Clonic convulsions of extremities started at day 2. Initial EEG performed at 10-day was reported as normal. Subsequently, myoclonus, which was easily induced by stimulation, was observed. Ictal EEG during myoclonus did not indicate that it was an electronical convulsion. Clonic convulsions were increased at 2 months of age when atypical suppression-burst pattern was transiently observed (Fig. 1A). Her seizures were controlled by combination of vitamin B6, zonisamide, phenobarbital, and KBr, but myoclonus continued. Brain magnetic resonance imaging (MRI) showed cortical atrophy and thin corpus callosum at 2 months of age (Fig. 1C–E). West syndrome was diagnosed at 5 months of age by intellectual disability without head control, series of tonic-spasms, and hypsarrhysmia on EEG (Fig. 1B).

MATERIALS AND METHODS

Molecular Cytogenetic Analysis

G-banded chromosomes of peripheral lymphocytes were analyzed. Fluorescence in situ hybridization (FISH) was performed using peripheral lymphocytes. Labeling, hybridization, wash, and image acquisition were performed as previously described [Saitsu et al., 2008]. RPCI-11 BAC clones and approximately 10-kb probes amplified by long PCR using LA Taq polymerase (Takara Bio, Otsu, Japan) were used as probes. Primer information is available on request.

GeneChip Human Mapping 250K *Nsp*I Array

Genomic DNA obtained from peripheral blood leukocytes were used for microarray analysis. Experimental procedures were performed according to the manufacturer's protocol with slight modification (fragmentation time was shortened to 25 min). Call rate was 89.5%. Copy number alterations were analyzed by using CNAG2.0 [Nannya et al., 2005].

Cloning of Translocation Breakpoints

The 1q32.1 translocation breakpoint was analyzed by Southern hybridization using *Eco*RI- and *Pst*I-digested patient DNA. Her parental DNAs were also analyzed. Probes were synthesized by PCR DIG probe synthesis kit (Roche, Basel, Switzerland) using RP11-134f21 DNA as a template. Primer information is available on request. Hybridization, washing and detection of probes were done according to the manufacturer's protocol. Images were captured on FluorChem (Alpha Innotech, San Leandro, CA). After identification of aberrant DNA fragments by Southern hybridization, size fractioning of electrophoresed *Eco*RI- and *Pst*I-digested DNA of the patient was performed using QIAEXII Gel extraction kit (Qiagen, Valencia, CA) in order to obtain der(1) and der(9) translocation junction fragments, respectively. The collected DNA was self-ligated by Ligation high (Toyobo, Osaka, Japan), ethanol precipitated and dissolved in 20 μl EB buffer (Qiagen). Inverse PCR was performed in 25 μl of volume, containing 2 μl ligated DNA, 1× LA PCR bufferII, 2.5 mM $MgCl_2$, 0.4 mM each dNTP, 0.5 μM each primer, and 1.25 U LA Taq polymerase (Takara Bio). Primers were listed below: *Eco*RI-forward, 5′-GAAATGGCCTGGCTTGGTTGCTAT-3′; *Eco*RI-reverse, 5′-CACTGAAGCTGCCCTTGAGAAGTGA-3′; *Pst*I-forward, 5′-TTTCCCTCCATGATTCCTCTCTGCT-3′; *Pst*I-reverse, 5′-CCAGGACAGCGTCTCACTCTCCATA-3′. Negative controls only used either forward or reverse primer. The PCR product was purified with ExoSAP (USB Co., Cleveland, OH) and sequenced for both forward and reverse strands with BigDye Terminator chemistry ver. 3 according to the standard protocol (Applied Biosystems, Foster city, CA). After breakpoint sequences were determined, breakpoint-specific primers for both der(1) and der(9) translocation junctions were designed: der(1)-forward, 5′-CCAAGGAATTGGGATCTCTGGGTCT -3′; der(1)-reverse, 5′-CATTCCATTCCATTCCCCTGCAC -3′ (1,098-bp);

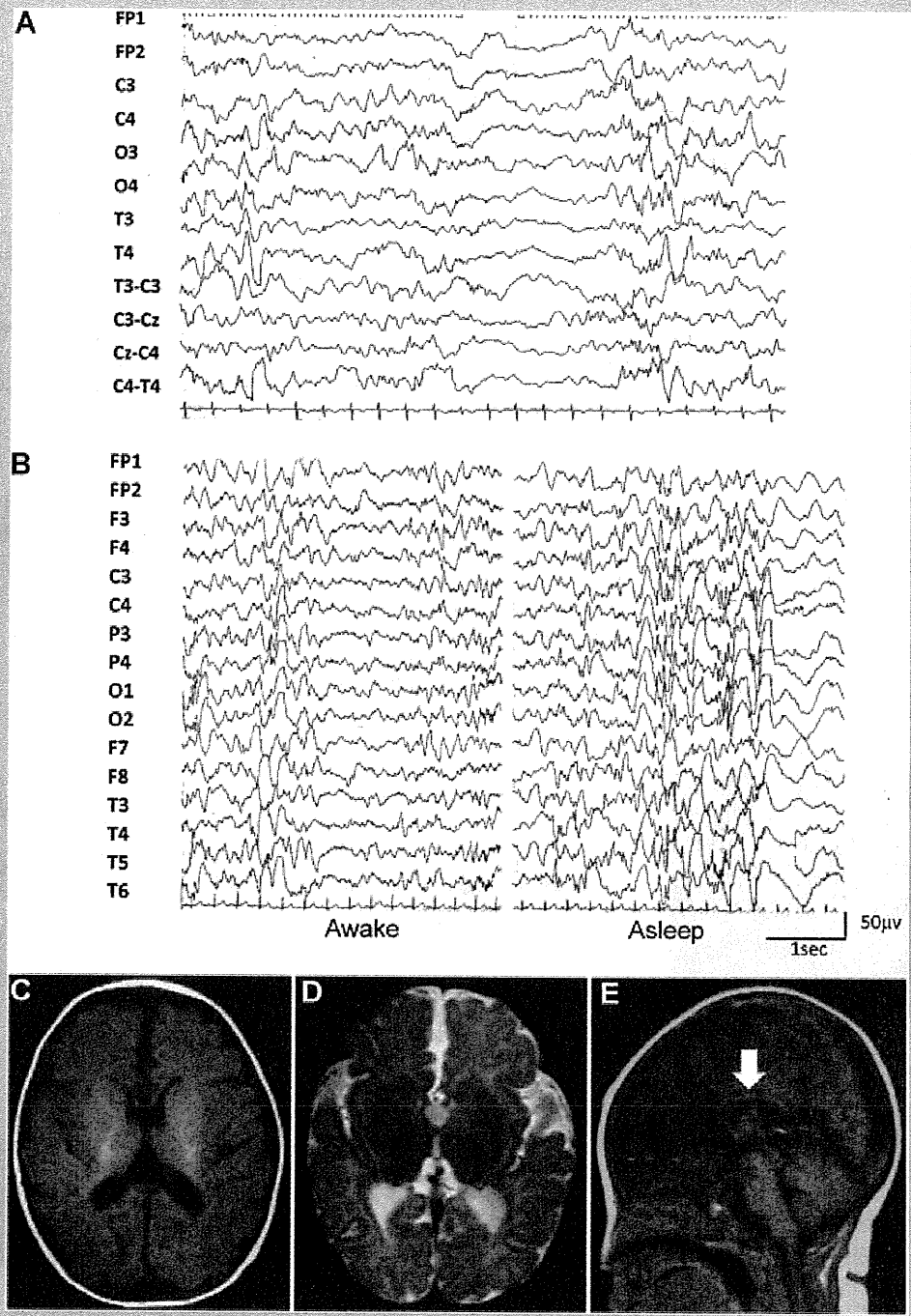

FIG. 1. EEG and brain MRI of the patient. A: Interictal high-voltage bursts alternate with low amplitude suppression phases at an approximately regular rate in both awake and asleep states at age of 2 months. Suppression phases do not exhibit "almost flat pattern" as typical suppression-burst pattern. B: Interictal EEG at 5 months shows multifocal spikes at awake (left), and high-voltage slow rhythm superimposed with irregular spikes; hypsarrhythmia at sleep with some periodicity (right). C,D: Brain MRI T1- (C) and T2-weighted (D) axial images show mild cortical atrophy with normal myelination. E: Sagital brain T1-weighted image shows thin corpus callosum (arrow)

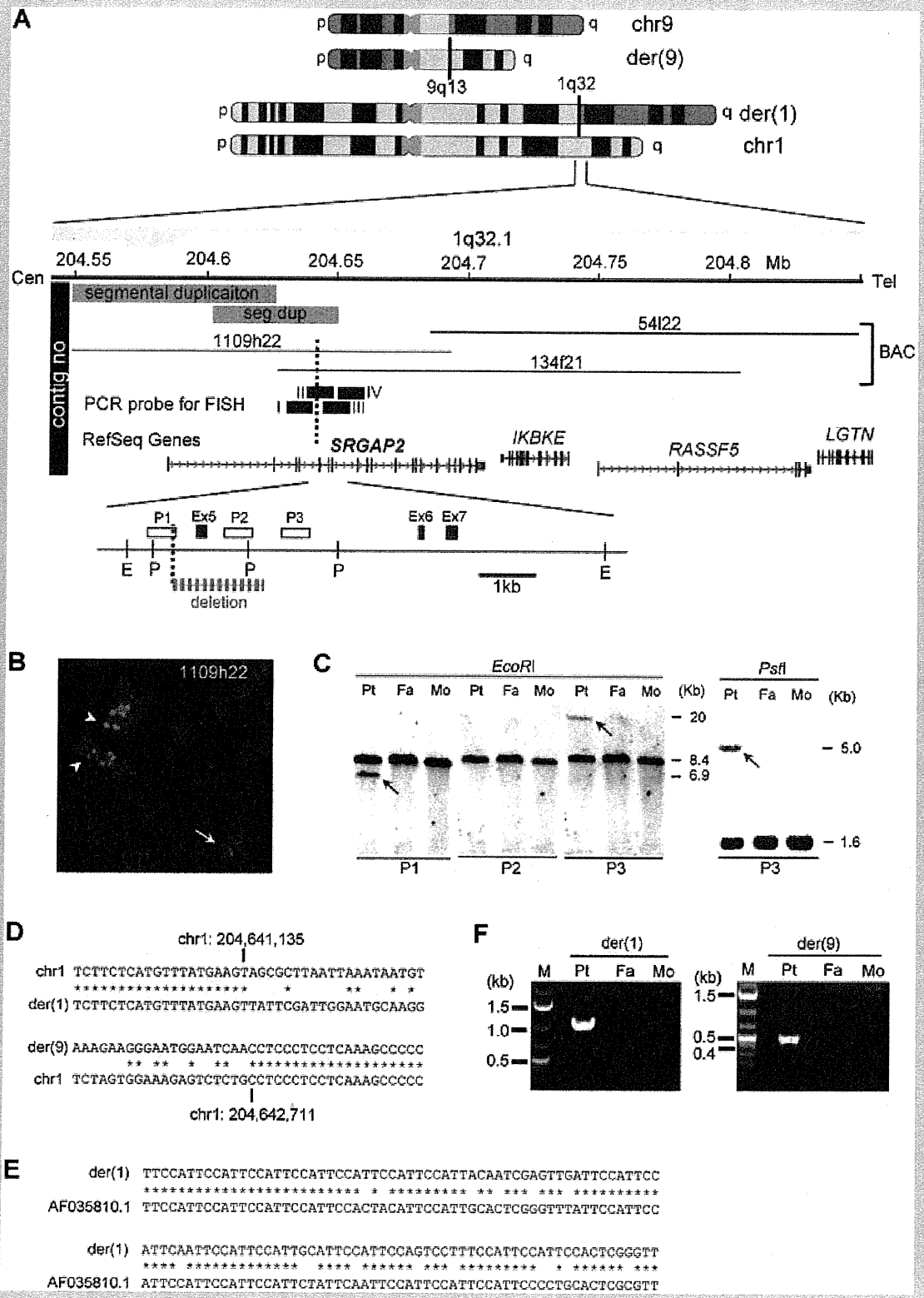
A
chr9
der(9)
9q13
1q32
der(1)
chr1
1q32.1
204.55
204.6
204.65
204.7
204.75
204.8 Mb
Cen
Tel
segmental duplicaiton
seg dup
contig no
1109h22
54l22
134f21
BAC
PCR probe for FISH
RefSeq Genes
SRGAP2
IKBKE
RASSF5
LGTN
P1
Ex5
P2
P3
Ex6
Ex7
deletion
1kb
B
1109h22
C
EcoRI
PstI
Pt Fa Mo Pt Fa Mo Pt Fa Mo (Kb)
Pt Fa Mo (Kb)
20
8.4
6.9
5.0
1.6
P1
P2
P3
P3
D
chr1: 204,641,135
chr1 TCTTCTCATGTTTATGAAGTAGCGCTTAATTAAATAATGT
der(1) TCTTCTCATGTTTATGAAGTTATTCGATTGGAATGCAAGG
der(9) AAAGAAGGGAATGGAATCAACCTCCCTCCTCAAAGCCCCC
chr1 TCTAGTGGAAAGAGTCTCTGCCTCCCTCCTCAAAGCCCCC
chr1: 204,642,711
F
der(1)
der(9)
M Pt Fa Mo
(kb)
1.5
1.0
0.5
0.4
E
der(1) TTCCATTCCATTCCATTCCATTCCATTCCATTACAATCGAGTTGATTCCATTCC
AF035810.1 TTCCATTCCATTCCATTCCATTCCACTACATTCCATTGCACTCGGGTTTATTCCATTCC
der(1) ATTCAATTCCATTCCATTGCATTCCATTCCAGTCCTTTCCATTCCATTCCACTCGGGTT
AF035810.1 ATTCCATTCCATTCCATTCTATTCAATTCCATTCCATTCCATTCCCCTGCACTCGCGTT